S

STM JOURNALS

Effect of Solar X-ray Flares on VLF Radio Wave Signal Strength at 19.8 and 24 kHz Received at Khatav (India) (16°46'N, 75°53'E)

A.K. Sharma[1], C.T. More[2],*
[1]Department of Physics, Shivaji University, Kolhapur, Maharashtra, India
[2]Department of Physics, Miraj Mahavidyalaya, Miraj, Maharashtra, India

Abstract
The period from August 2009 to July 2012 was an important period as 2009–10 was solar minimum period, and solar cycle was extended by 16 months during this period. In this period, solar activity like solar X-ray flares, solar wind, coronal mass ejections were at minimum level. In this research, it is focused on detailed study of response of signal strength of VLF radio waves transmitted by VLF station NWC Australia (19.8 kHz) and VLF station NAA, America (24 kHz) to the solar flares. This study explores how the ionosphere and VLF radio waves react to the solar flares. In case of NWC (19.8 kHz), the signal strength recording shows very nice SID peaks. In case of VLF signal transmitted by NAA at 24 kHz, the average SID peaks are observed. The two frequencies signals are recorded for four years.

Keywords: VLF signal strength, solar flares, sudden ionospheric disturbance, signal perturbation solar flare intensity

***Author for Correspondence** E-mail: chandrakantmore136@yahoo.co.in*

INTRODUCTION
A solar flare is a giant explosion on the surface of the sun mostly near sunspots. It is defined as a sudden, rapid, and intense variation in brightness. It occurs when magnetic energy built up in the solar atmosphere is suddenly released. Radiation is emitted across the entire electromagnetic spectrum, from radio waves at the long wavelength end, through optical emission to X-rays and gamma rays at the short wavelength end. Solar flares occur most when the Sun is active in the years around solar maximum. Many solar flares can occur on just one day during this period. Around solar minimum, solar flares might occur less than once per week. Large flares are less frequent than smaller ones. Some (mostly stronger) solar flares are known to produce so called coronal mass ejections which can lead to geomagnetic storms when they are directed towards earth.

THE CLASSIFICATION OF SOLAR FLARES
Solar flares are classified as A, B, C, M or X according to the peak flux (in watts per square meter, W/m^2) of 1 to 8 Angstroms X-rays near earth, as measured by XRS instrument on-board the GOES-15 satellite which is in a geostationary orbit over the Pacific Ocean. The different solar flare classes are A, B, C, M and X. Each X-ray class category is divided into a logarithmic scale from 1 to 9, for example, B1 to B9, C1 to C9, etc. An X2 flare is twice as powerful as an X1 flare, and is four times more powerful than an M5 flare. The X-class category is slightly different and doesn't stop at X9 but continues on. Solar flares of X10 or stronger are sometimes also called Super X-class solar flares.

X-CLASS SOLAR FLARES
X-class solar flares are the biggest and strongest solar flares. Such solar flares occur about 10 times in an average per year [1–3]. These flares occur during solar maximum period than the solar minimum period. These flares produce strong to extreme radio blackouts on the daylight side of the earth. These flares produce strong and long lasting solar radiation storm and release a significant coronal mass ejection when the solar flare emitted from the center of the earth-facing solar surface. These flares cause severe to extreme geomagnetic storming on earth. The

X-class continues after X9 are called as super X-class solar flares. Solar flares of X10 class are very rare and occur only a few times during the 11 year solar cycle [4, 5]. It is a good thing that these powerful X10 solar flares do not occur frequently. The coronal mass ejections which are erupted from X10 solar flares are able to cause severe damage to the satellites and power lines. The satellites started to measure the energies of the solar flares since 1976. The largest solar flare recorded since 1976 was X28 solar flare which occurred on November 4th, 2003 during solar cycle 23[6]. A good thing for us was that the sunspot group which produced this solar flare had already rotated largely of the earth-facing solar disk when the X28 solar flare occurred.

SOLAR FLARE INTENSITY

The intensity of solar flares can be measured by many methods. The X-ray classification of solar radiation at present measures the maximum flux of X-rays having wavelength ranging from 0.1 to 0.8 nanometer that produced by the flare. The approximate X-ray flux is indicated by the letters A, B, C, M, or X. The A class flare is the weakest flares and X class flare is the strongest flare, the letters C, M, and X stand for common flare, medium flare, and xtreme flare. Numbers after the letter, such as in C4.2 or X2.2, measure the X-ray flux more precisely according to the Table 1.

Table 1: X-ray Flare Intensity [1].

X-ray Flare Class	X-Ray Flux (W/m^2)	X-Ray Flux ($erg/cm^2 \cdot s$)
An	$n \times 10^{-8}$	$n \times 10^{-5}$
Bn	$n \times 10^{-7}$	$n \times 10^{-4}$
Cn	$n \times 10^{-6}$	$n \times 10^{-3}$
Mn	$n \times 10^{-5}$	$n \times 10^{-2}$
Xn	$n \times 10^{-4}$	$n \times 10^{-1}$

If typical value of X-ray flux is M2.8 then it is equal to 2.8×10^{-5} W/m^2; X2.2 $= 2.2 \times 10^{-4}$ W/m^2 C2.5$= 2.5 \times 10^{-6}$ W/m^2. For the flare classes A, B, C, and M, the value of *n* is in between 1.0 and 9.9, but for X class the value of *n* can be more than 9.9 as needed. Sudden brightening observed on the solar limb during solar flare emission, which gives large energy release of the order of 6×10^{25} joules [3, 4]. During the flare, clouds of electrons, ions, and atoms are ejected through the solar corona into the space. These particle clouds reach the earth in a one day or in two days after the event took place. The flares that occur in other stars are termed as stellar flares [5].

Solar flares effects on the solar photosphere, chromospheres, and corona when plasma medium is heated to some tens of millions of Kelvin's and thereby electrons, protons, and heavier ions are accelerated near to the speed of light [7]. They produce all types of radiation across the electromagnetic spectrum of all wavelengths ranging from radio rays to gamma rays although, large part of the energy goes to the frequencies outside the visual band. And hence the most of the flares are not visible to our eye. These flares can be made visible by using special instruments. The intense magnetic field is generated on sun's surface. This region produces flares in active regions near to the sunspots, where flares penetrate the photosphere to link the solar corona to the solar interior. X-ray flares are powered by the sudden release of magnetic energy which is stored in the solar corona. The time duration of flares is minutes to hours. This magnetic energy may produce coronal mass ejections (CME) from the solar surface. Although the relation between the coronal mass ejections (CMEs) and solar X-ray flares are still not well understood. Research is being done to understand this relationship.

FIELD STRENGTH DATA OF VLF RADIO WAVES At 19.8 AND 24 kHz

The VLF field strength monitoring system at Khatav, India (16°46' N, 75°53' E) is shown in Figure 1. Experimental set up -Two Channel VLF Field Strength Monitoring System is shown in Figure 2. Figure 3 (a) and (b) shows Loop Antennas.

VLF signal of 19.8 kHz from NWC Cape North, Australia is continuously being recorded by SID monitoring system since April 2007. VLF signal shows characteristic variation in diurnal and seasonal field strength. It has been observed that VLF solar flares are huge explosions in the sun's atmosphere. These solar flares appear to our instruments as bright flashes in the visible light followed by a huge burst of high-energetic protons and solar radiation. Moreover their characteristics can

include burst of radio waves, EUV and X-rays [1, 8]. A large solar flare can release a thousand million megatons of energy (more precisely 10^{28} to 10^{34} ergs) in a single explosion. The released energy is transformed into the following types:

1. Thermal energy leading to an increased brightness of e.g. the Hα and X-ray emission,
2. Particle kinetic energy leading to the acceleration of electrons to energies of 10 KeV to 1 GeV and ions to energies from a few MeV to GeV.

3. Mechanical energy leading to several kinds of plasma ejection. Solar flares sometimes occur together with other signatures of solar activities e.g. prominence eruptions, CME's and interplanetary shock waves. However the exact relationship between these phenomena is not yet completely understood [1]. The effect of solar activity like Solar X-ray flares on VLF radio wave propagation can be studied by using VLF field strength monitoring system.
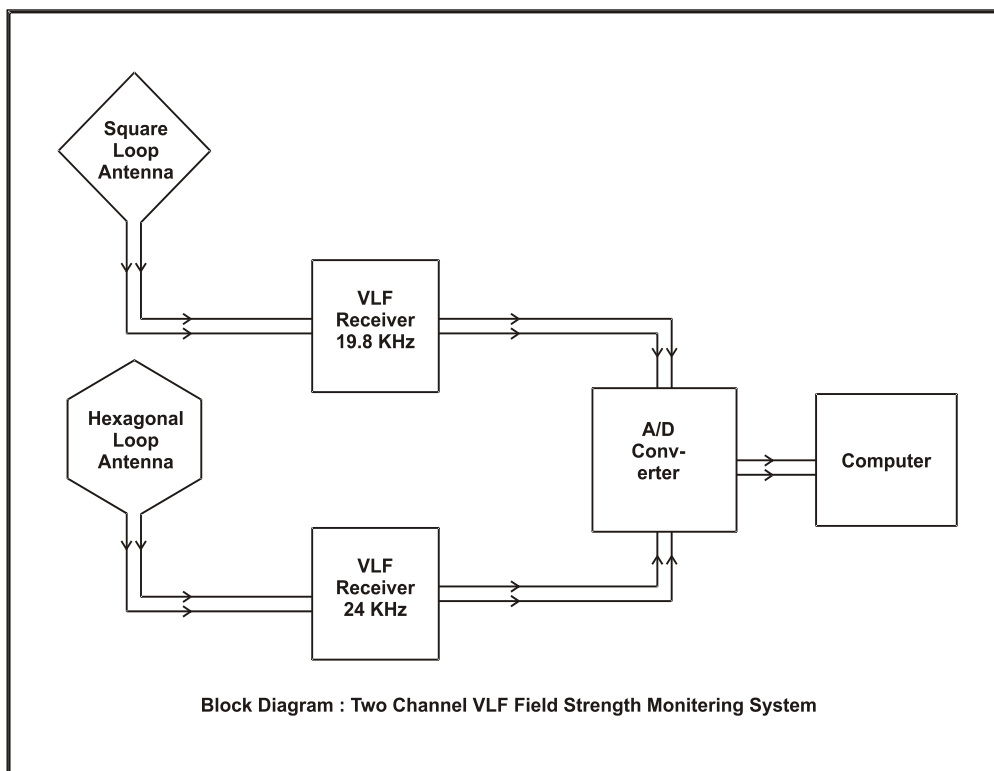

Fig. 1: Block Diagram of VLF Field Strength Monitoring System which Consists of Loop Antennas, SID Monitor, A/D Converter and Computer.

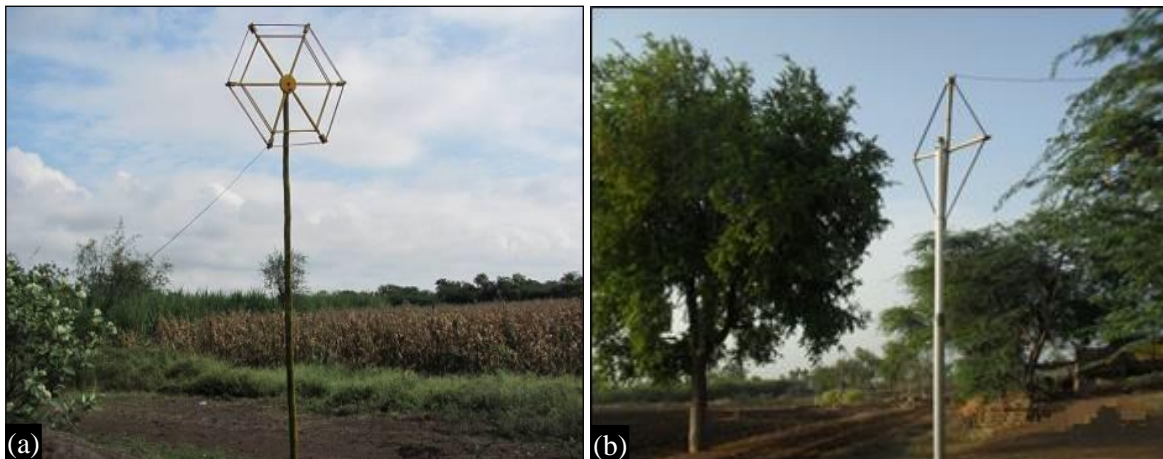*Fig. 2: Experimental Set up -Two Channel VLF Field Strength Monitoring System.*

Fig. 3: Loop Antennas: (a) Hexagonal Loop Antenna (b) Square Loop Antenna.

DATA ANALYSIS

VLF signal from transmitter, emitted with well stabilized field strength, propagating under undisturbed ionospheric conditions, is continuously being recorded by VLF field strength monitoring system since April 2007, shows the characteristic field strength as well as diurnal and seasonal variation [9–11]. The most prominent change in the earth-ionosphere waveguide take place during the day-to-night and also in reverse mode i.e. night to day change [12]. But due to solar X-ray flares significant modifications of the propagating conditions happen due to significant changes in the lower ionosphere electron density [13]. Although the solar rays having wavelength 1215.67 Å is main source of ionization. These Lyman-α emission is enhanced during the flare event, the X-ray emission overwhelms its effect several times leading to the increase in the D-layer electron density by 1–2 orders of magnitude [14, 15]. Enhanced D-layer density causes the change in the electrical conductivity at the upper waveguide edge along the trace of the VLF signal and consequently, gives rise to the change in all propagating parameters. These changes are clearly detected in the form of VLF field strength variation. Although flare effects on the VLF signal are always well recognizable, they can vary substantially along different signal traces. The theory of VLF propagation through the earth-ionosphere waveguide, at regular (quiet) ionospheric conditions, is well established [16, 17]. When solar flares occur, sudden energy bursts in the X-ray domain appear most distinctly impressed on the VLF signal, amplitude with an abrupt increase, followed by the subsequent signal recovery within time intervals (typically less than an hour), which correspond to flare duration [1,10]. Over 50 flare events are detected during the period of July 1, 2009 to July 30, 2010.

Though apparently different depending on the path, the flare induced VLF disturbances show stable patterns while amplitude enhancement on long NWC path is regularly detected. We relate the VLF signal variations measured by the VLF field strength monitoring system to the solar X-ray irradiance, as monitored by the GOES 12 satellite. Figures 4 and 5 gives representative example of flare-induced field strength variations, measured for the NWC signal, on the active day of December 22 and December 23, 2009. Figure 5 shows the unperturbed average plot of field strength of the month of December 2009 is overlapped with the plot of disturbed day December 23, 2009. The Figure 6 shows EUV image of the sun on December 23, 2009.

This perturbation is observed due to C-class solar X-ray flare. The correspondence between the X-ray flare events detected by GOES 12 satellite enhancement is remarkable; moreover, the field strength response to the flare is clearly present [20–22]. X-ray irradiance have a distinct impact upon VLF field strength characteristic, which display different patterns peculiar to the NWC path, throughout a single active day.

When a solar flare occurs, then there is an increase the ionization of all the layers

including the D-layer. Thus D-layer becomes strong enough to reflect the VLF radio waves at a lower altitude. So during a solar flare, the waves travel less path (reflecting from D-layer instead from E or F-layer). The signal strength usually increases because the wave does not lose energy as it reflects from bottom of the D-layer [23]. However, the VLF signal strength during flare can sometimes decrease. The signal strength could decrease because destructive interferences of waves due to different path. The lower the waves reflect, the more collisions, or interferences of waves there will be because of the thicker atmosphere. These collisions of waves can result in destructive interference (Figure 7).
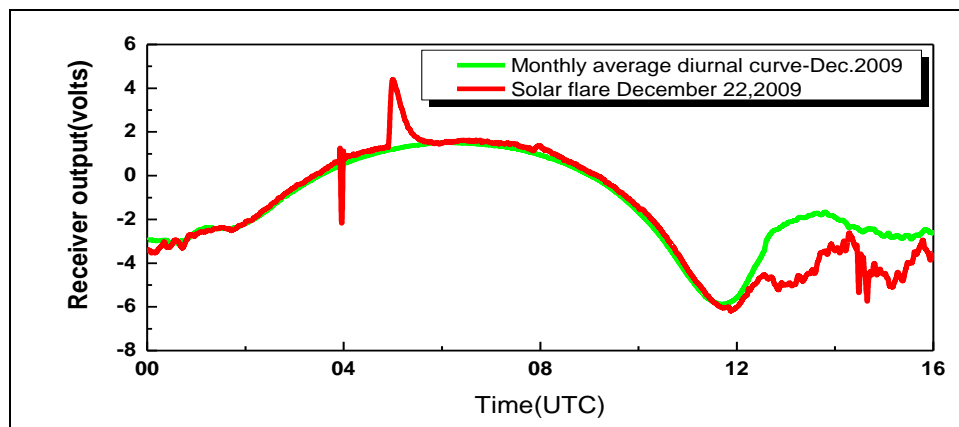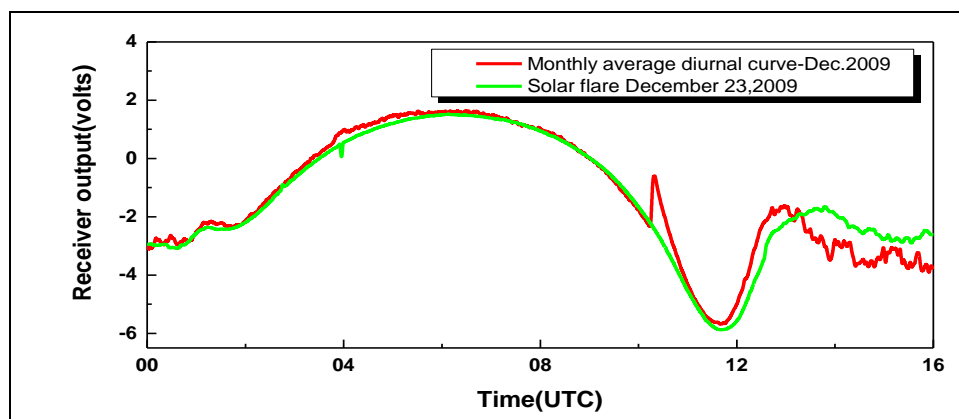

***Fig. 4:** C-Class Solar Flare, December 22, 2009.*

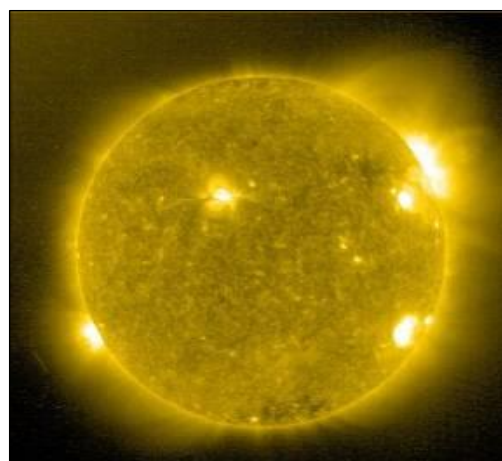***Fig. 5:** C-5 Class Solar X-ray Flares Occurred on December 23, 2009.*

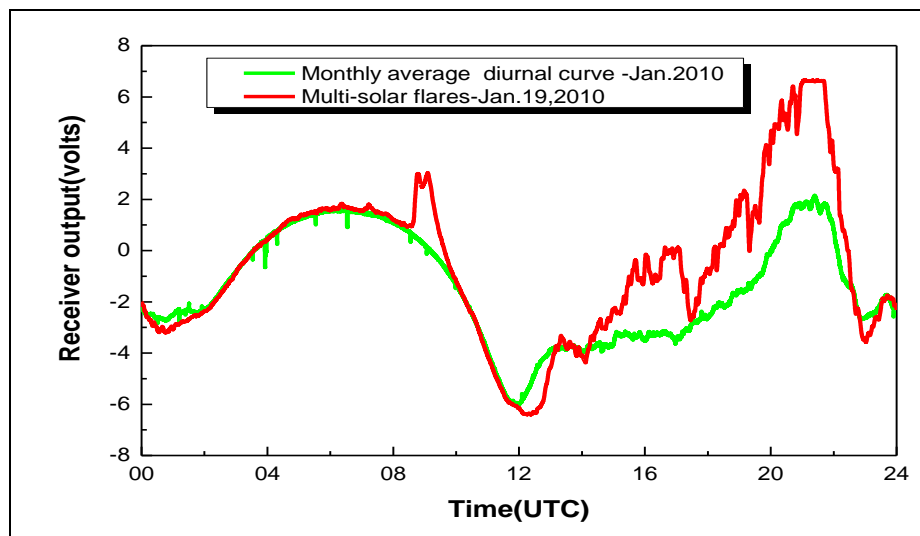***Fig. 6:** Sun Image in EUV, December 23, 2009[19].*

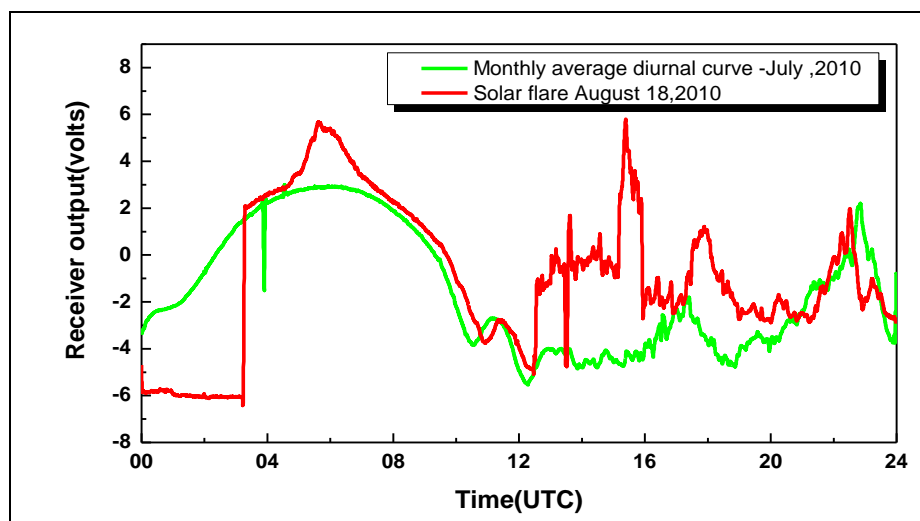**Fig. 7:** *Solar X-ray Flares on January 19, 2010.*

Fig. 8: *GOES X-Ray Data on August 18, 2010.*

As soon as X-ray flares end, the sudden ionospheric disturbance (SID) ends as the electron density in the D-layer rapidly return to normal as a result of attachment and /or recombination process. The VLF field strength monitoring system has also recorded many B-Class solar X-ray flare events along with those of M and X-class. The plot of signal strength against time recorded on December 22, 2009 can be compared with the GOES satellite data graphs [24]. We can also confirm the H-alpha line images of the sun on the same day and correlate the event and X- ray flare (Figure 8). We can also do correlation study between the sunspots and solar X-ray flares. Ionosphere of the earth is an important ground based tool to study solar X-ray flares and also their effects on ionospheric VLF radio propagation.

Multiple Flare Analysis

For the analysis of VLF data, the series of flares are selected that had occurred on January 20, 2010 and it is presented, along with the average VLF field strength measurements in Figure 9. The reasons for this choice are as follows:

1. The flare intensity ranging from class C to X is characteristic for the majority of the flares that have been VLF recorded at Khatav (India) on this active day.
2. As many SIDs in the form of signal enhancements overlapping in occurrence due to multiple solar X-ray flares have been recorded on this day from sunrise to sunset.

Figure 10 shows overlapping curves of solar X-ray flares detected by VLF Monitoring

Research & Reviews: Journal of Space Science & Technology
Volume 6, Issue 3
ISSN: 2321-2837 (Online), ISSN: 2321-6506 (Print)

STM JOURNALS

system and GOES satellite on active day of January 20, 2010. It is observed that solar X-ray flare events started to occur from January 18, 2010 and these solar activity ends on January 21, 2010. Figure 11 shows solar flare on January 20, 2010 on solar limb. Figure 12 shows UV image of the sun on January 21, 2010. It shows solar flares. It is also observed that many M-class and C-class solar X-ray flares have been occurred during this period.
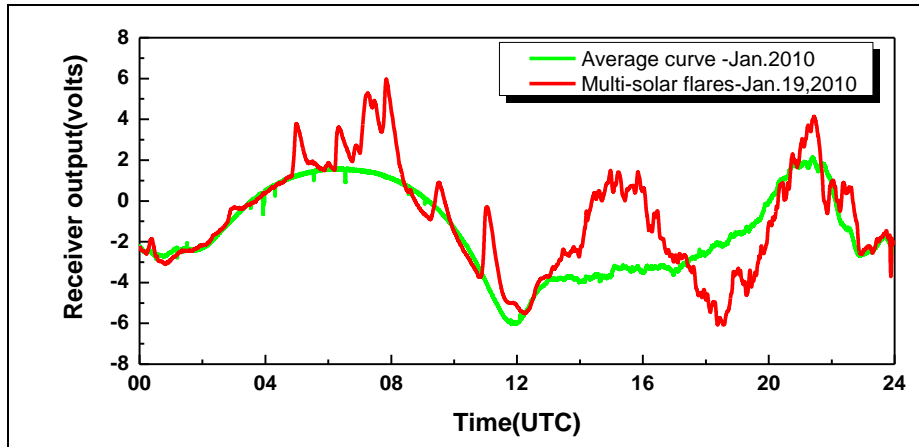

Fig. 9: *Solar X-ray Flares on January 19, 2010 Recorded at 19.8 kHz (NWC).*
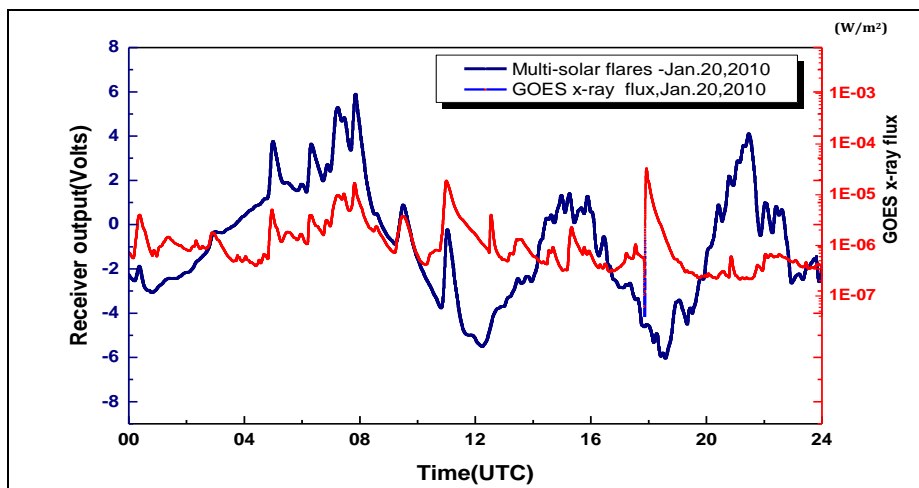

Fig. 10: *Overlapping Curves of Solar X-Ray Flares Detected by VLF Monitoring System and GOES Satellite on January 20, 2010.*
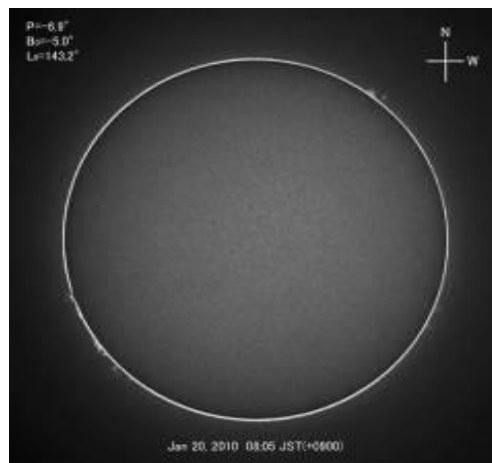

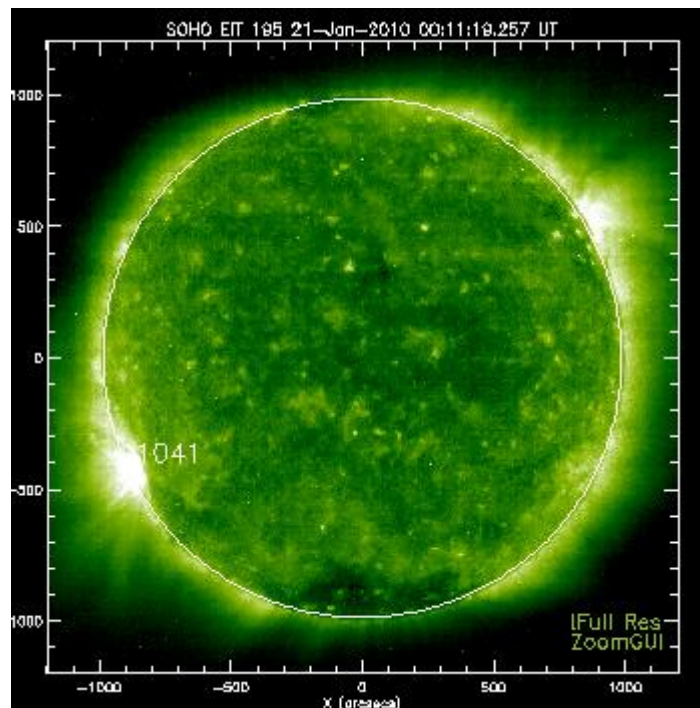**Fig. 11:** *Solar X-Ray Flares Images of Sun on January 20, 2010 [25].*

Fig. 12: *Solar X-Ray Flares Images of Sun on January 21, 2010 [25].*

Table 2: *Measured Field Strength Variation at Different Stages of Flare Occurrence and at Different Angle of Elevation and Intensity of X-Ray Flares on January 20, 2010.*

Flare No.	Flare Time (UT)			Duration (Minutes)	V_f (Volts)	V_q (Volts)	ΔV (Volts	Class of flare	Flare Intensity (W/m²)
	Start	Max	End						
1	00.13	00.23	00.30	17	4.825	4.11	0.715	C4	4×10^{-6}
2	02.49	02.58	03.13	24	6.44	3.81	2.63	C1	1×10^{-6}
3	04.50	04.58	05.22	32	10.47	8.01	2.46	C1	1×10^{-6}
4	05.51	06.00	06.11	20	8.536	8.27	0.266	C6	6×10^{-6}
5	06.13	06.20	06.46	33	10.255	8.24	2.015	C5	5×10^{-6}
6	06.46	06.53	07.00	14	9.571	8.21	1.361	C7	7×10^{-6}
7	07.00	07.16	07.23	23	12.169	8.14	4.029	C8	8×10^{-6}
8	07.23	07.28	07.41	18	11.72	8.05	3.67	C9	9×10^{-6}
9	07.41	07.51	08.33	52	12.618	7.79	4.828	M1	1×10^{-5}
10	08.33	08.39	08.46	13	7.305	7.091	0.214	C2	2×10^{-6}
11	09.15	09.30	10.01	46	7.55	5.821	1.729	C5	5×10^{-6}
12	10.50	11.03	11.38	48	6.387	1.94	4.447	M2	2×10^{-5}

The characteristics of the flare events are given in Table 2. Table 2 shows measured field strength variation at different stages of flare occurrence and at different angle of elevation and intensity of X-ray flares for January 20, 2010. The first column identifies the flare number the second column lists the time at which the characteristic feature of the field strength variation (minimum/maximum) is detected.

The third column shows the duration of events. Next column four shows the output voltage of detector when flare occurred and column five shows the average detector output voltage for the month of January 2010. The column six shows variation ΔV in detector output. The column seven shows the Class of flare and the last column shows the flare intensity (W/m²) as the data recorded by satellite GOES 12.

Determination of Field Strength Variation ΔV Due to X-ray Flares

From Figure 13, field strength variation ΔV is determined from the VLF field strength measurements on the quiet day V_q, and that due to X-ray flare V_f. It is given by $\{\Delta V\} = \{V_f - V_q\}$ it can be seen from Table 2 that the smallest enhancement in field strength (as measured by the detector output) is 0.214 Volts and largest one is 4.828 Volts. However, amount of field strength enhancement depends upon the intensity of X-ray flux and solar elevation angle. If the detector output voltage is divided by amplification factor of the receiver, one can get field strength variation at the receiver input terminal. Thus, it is clear that our SID Monitor (VLF field strength monitoring system) is very sensitive and can detect small solar flares as B class.

Some small medium and large solar flares are shown in Figures 14–23. Figure 14 shows overlapping curves of solar X-ray flares detected by VLF monitoring system at 19.8 kHz and 24 kHz on December 22, 2009. This is C 7.2 solar flare which started to disturb the D-region of the ionosphere at 4.25 UTC and ends at 5.22 UTC. The signal strength of NWC started to increase from its value 1.23 Volts to its maximum value 4.56 Volts. The signal strength variation for this flare was 3.29 Volts. This variation for NAA at 24 kHz was

different. The NAA signal started to increase from its minimum value -3.965 Volts to its maximum value -1.758 Volts. The signal strength variation for this flare for NAA was 1.207 Volts. It shows that the signal strength variation for NWC signal is observed to be more than that of NAA signal. Figure 15 shows overlapping curves of solar X-ray flares detected by VLF monitoring system at 19.8 kHz and 24 kHz on February 16, 2011. On this day there were multi-flares which started to disturb the ionosphere at 1.03 UTC and ends at 7.16 UTC. From the Figure 15, it is observed that as the intensity of X-ray flux increases, then there is increase in signal strength variation. Figure 16 shows overlapping curves of solar X-ray flares detected by VLF Monitoring system at 19.8 kHz of NWC and 24 kHz of NAA on March 8, 2011. As far as the intensity of solar X-ray flux is concerned, Figure 17 is very important. During this recording, GOES data is not available for the period from 5.16 UTC to 6.32 UTC. During the same period, NWC signal have been recorded solar flare. From the analysis, the intensity of this solar flare is estimated to be equal to 5.34×10^{-5} (Figure 24). Figure 17 shows overlapping curves of solar X-ray flares detected by VLF Monitoring system and solar X-ray flux recorded by GOES Satellite on September 23, 2011.
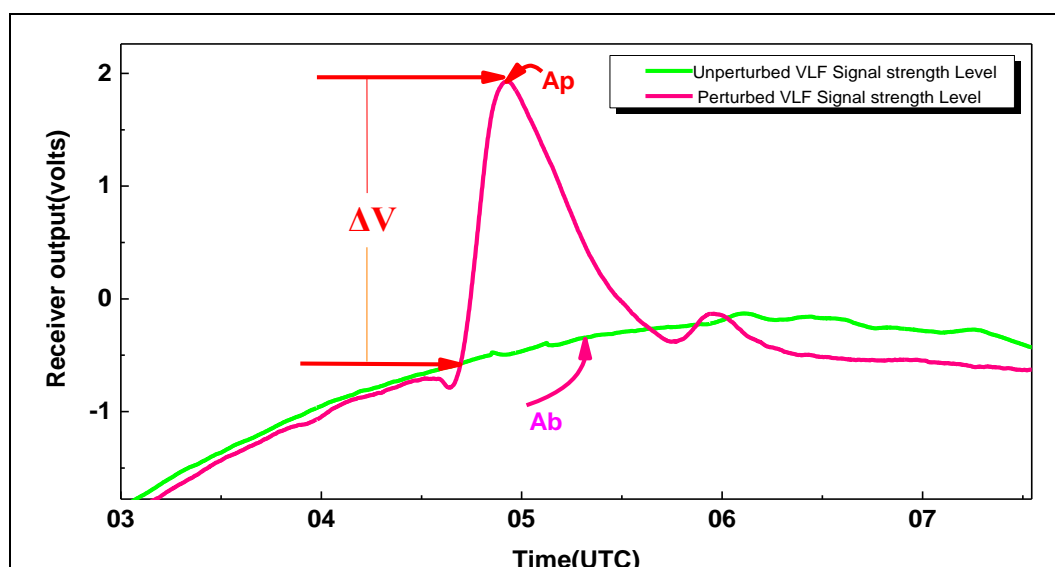
Fig. 13: Method of Determining Perturbation (Enhancement) in Amplitude of VLF Signals During Solar Flare.

Fig. 14: *Overlapping Curves of Solar X-Ray Flares Detected by VLF Monitoring System at 19.8 kHz NWC and 24 kHz NAA on December 22, 2009.*

Fig. 15: *Overlapping Curves of Solar X-Ray Flares Detected by VLF Monitoring System at 19.8 kHz NWC and 24 kHz NAA on February 16, 2011.*

Fig. 16: *Overlapping Curves of Solar X-ray Flares Detected by VLF Monitoring System at 19.8 kHz NWC and 24 kHz NAA on March 8, 2011.*

Fig. 17: *Overlapping Curves of Solar X-Ray Flares Detected by VLF Monitoring System and Solar X-ray flux Recorded by GOES Satellite on September 23, 2011.*
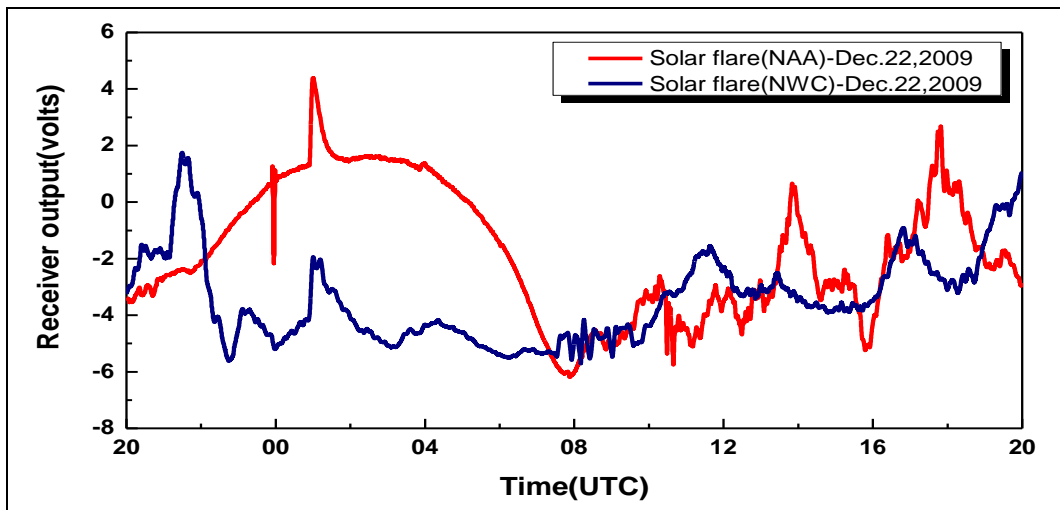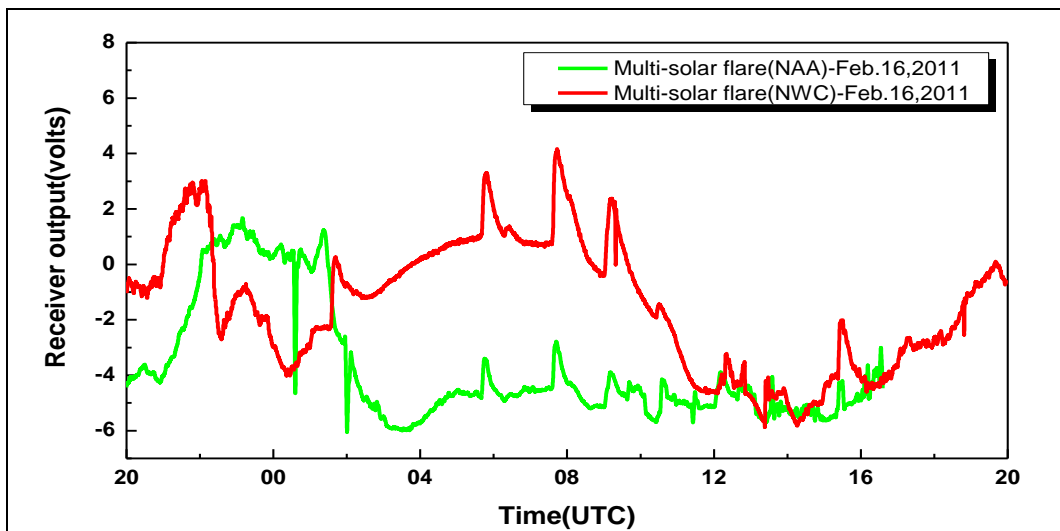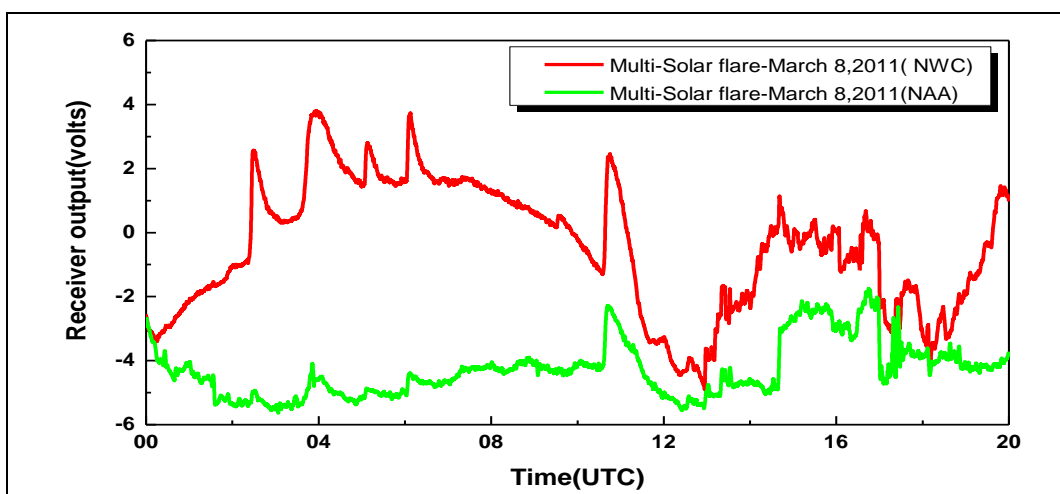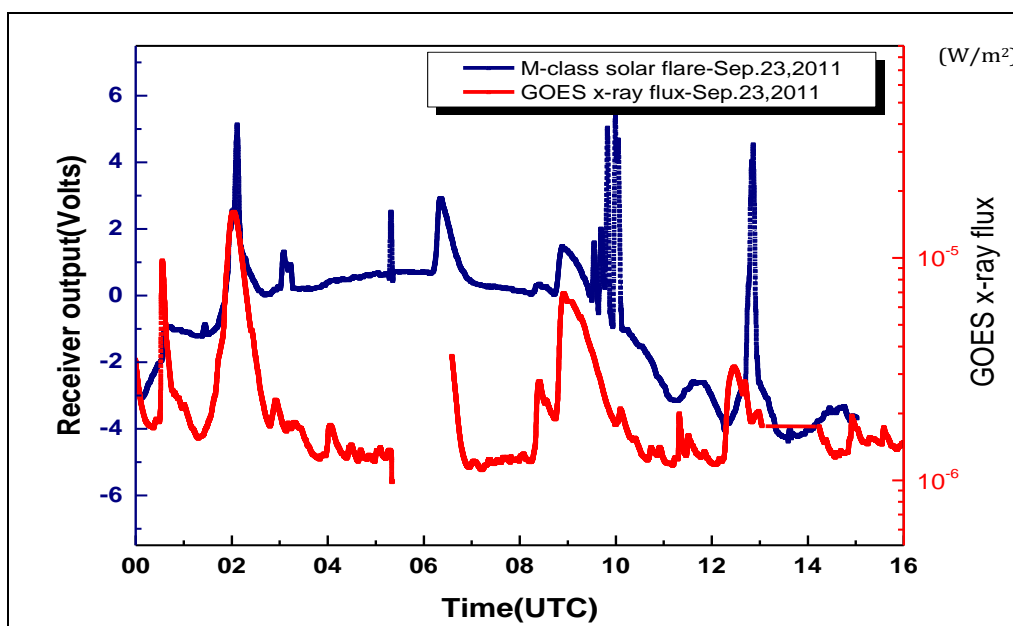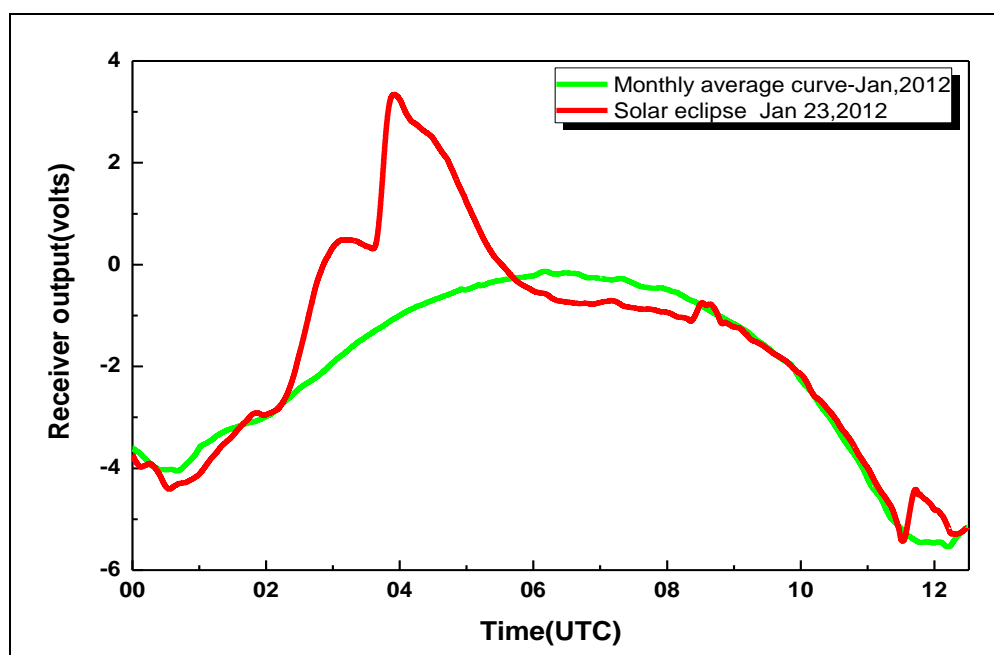

Fig. 18: *NWC Signal Strength Variation for Solar X-Ray Flares on January 23, 2012.*

The Figure 18 shows solar X-ray flares on January 23, 2012. This flare is of different type. Initially, the first flare started to increase the signal strength from -4.29 Volts to its maximum value at -3 Volts. This first flare was of C1.9. But there is another solar flare burst and due to that signal strength started again to increase up to 0.4 Volts. The total signal strength variation was 3.34 Volts. Due to this flare the ionosphere remained disturbed for a long time.

Another interesting solar flare has been recorded and it can be seen along with solar X-ray flux on January 26, 2012. It is shown in Figure 19. Figure 20 shows overlapping curves of X-class solar X-ray flares detected by VLF monitoring system and GOES satellite with unperturbed day on February 15, 2011.

The NWC signal strength varies from -1.76 up to 5.85 and overall variation in signal strength

is 7.61 Volts. This much variation is due to X2.2 solar flare.

On August 9, 2011, the biggest solar flare of the 24th solar was observed. The NWC signal strength varies for first M2.5 solar flare from 0.09 Volts up to 5.30 Volts. The signal strength variation is 5.21 Volts. The biggest solar flare observed was X6.9 and this flare caused the NWC signal strength variation up to 5.56 Volts. Figure 22 shows overlapping curves of solar X-ray flares detected by VLF Monitoring system and GOES Satellite X-ray flux data on September 22, 2011. The signal strength of NWC transmitter varies for X1.4 solar flare is 4.74 Volts. During the daytime there was a GOES satellite X-ray receiver was off for the period from 5.20 UTC to 6.20 UTC. During this time our VLF field strength monitoring system has recorded solar flare.

Fig. 19: *Overlapping Curves of Solar X-ray Flares Detected by VLF Monitoring System and GOES Satellite on January 26, 2012.*

Fig. 20: *Overlapping Curves of Solar X-ray Flares Detected by VLF Monitoring System and GOES Satellite with Unperturbed Day on February 15, 2011.*

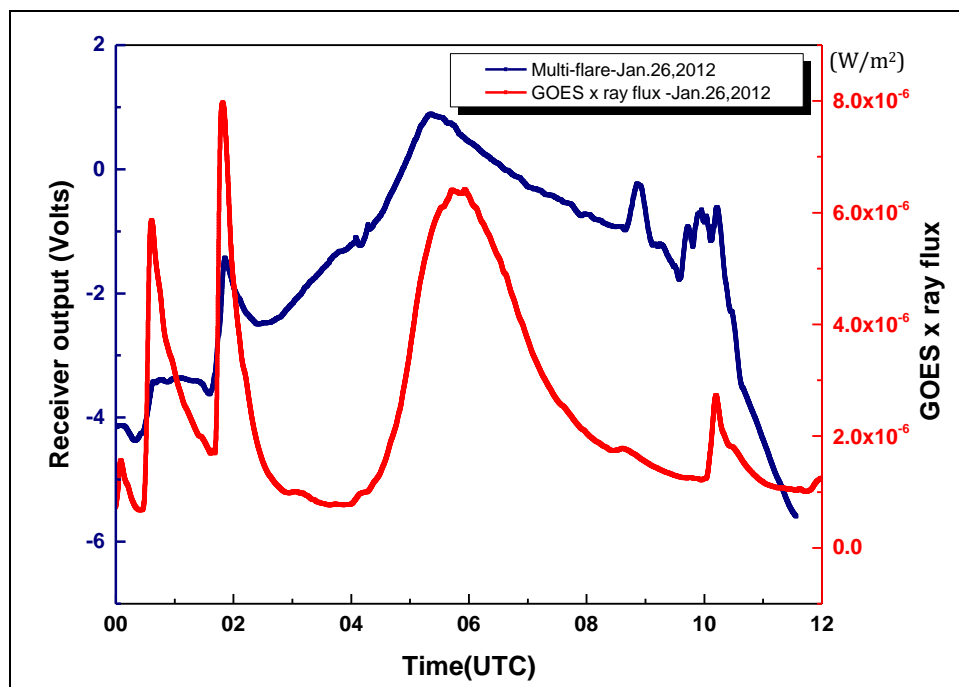***Fig. 21:*** *Overlapping Curves of Solar X-ray Flares Detected by VLF Monitoring System and GOES Satellite on August 9, 2011.*
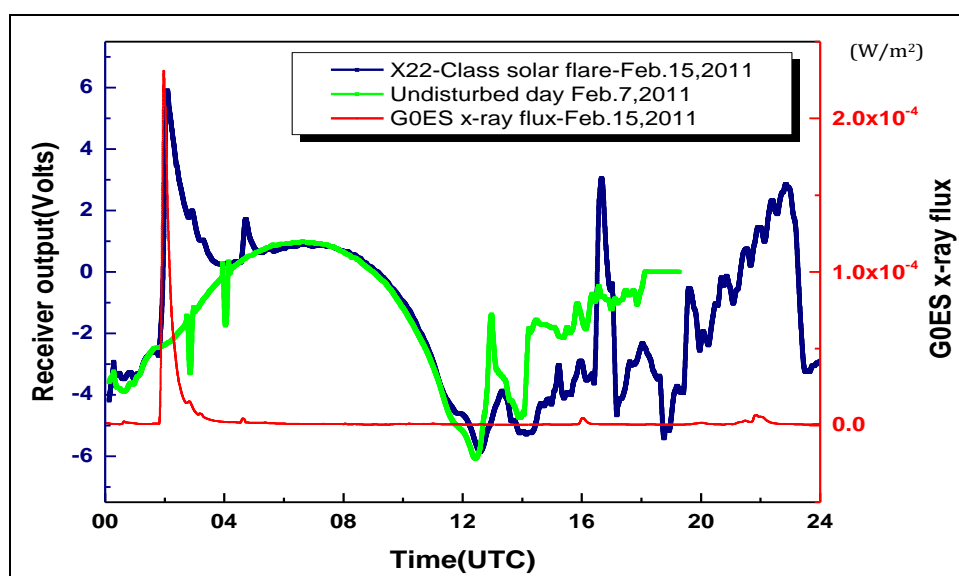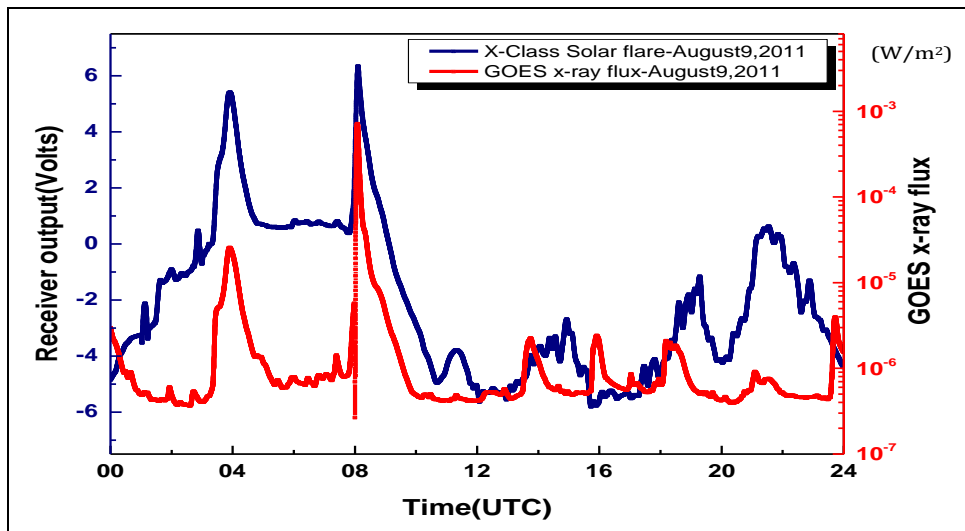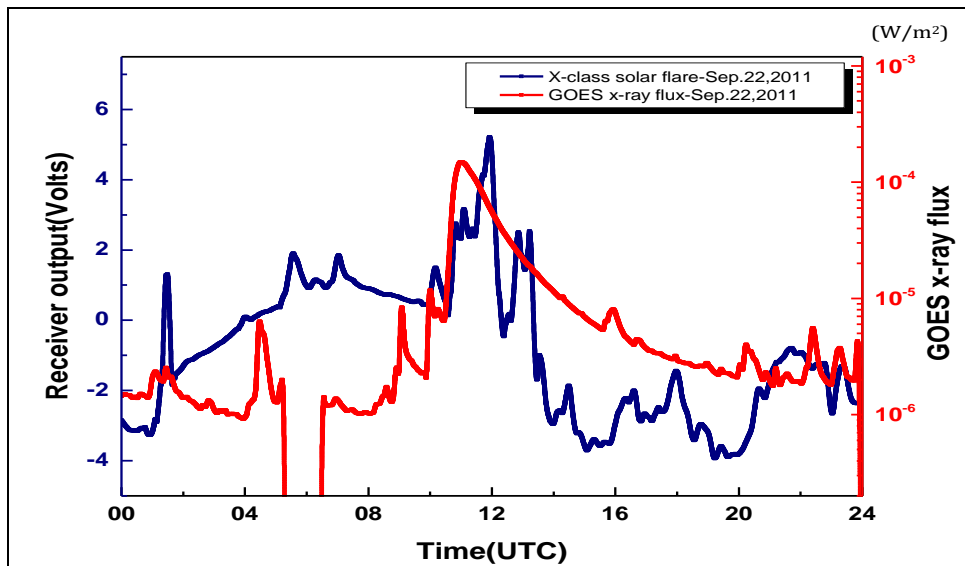

Fig. 22: *Overlapping Curves of Solar X-Ray Flares Detected by VLF Monitoring System and GOES Satellite with Unperturbed Day on September 22, 2011.*
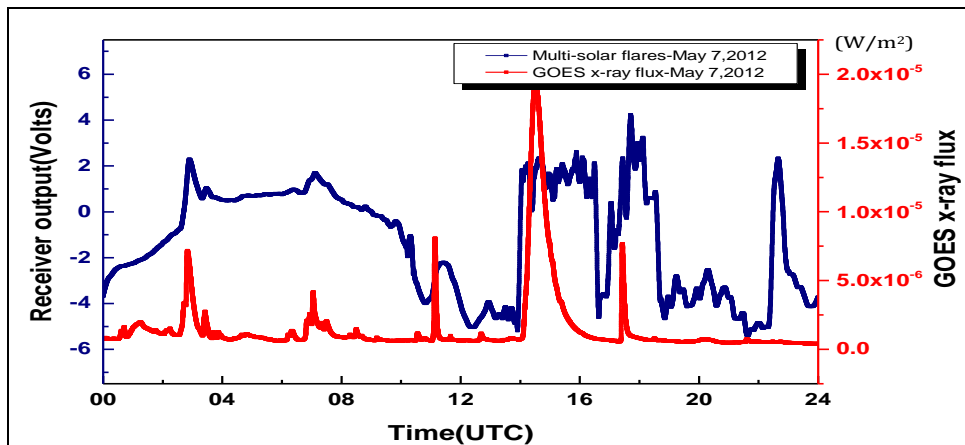

Fig. 23: *Overlapping Curves of Solar X-Ray Flares Detected by VLF Monitoring System and GOES Satellite on May 7, 2012.*

The signal strength of NWC transmitter is observed to be varied during night time. It is observed on May 7, 2012. The Figure 23 shows the corresponding overlapping curve of NWC signal strength and GOES X-ray flux for C and M class solar flares. The M class flare started at 14 UTC and ends on 14.31 UTC during nighttime. It indicates the effect of solar flare on VLF signal strength during nighttime. This signal strength variation is observed for only M-Class or bigger than that flares.

RELATIONSHIP BETWEEN SIGNAL PERTURBATION AND SOLAR FLARE INTENSITY

In the daytime, the VLF signals are smooth. This can be explained that the ionospheric D-region is formed by Lyman-α emission which ionizes the NO. The ionization of X-ray flare is more significant than that of the cosmic rays and Lyman-α emission. This leads to enhance the electron density profile which increases more smoothly with height in the disturbance condition than that in the normal condition [1, 26–28]. The ionospheric boundary becomes more conductive, hence the VLF signals reflect better at D-region. From Aug 2009 to May 2012, observing the responses of NWC and NAA during the solar flares and it is observed that there is a time delay is about 1– 15 min. In some special cases, it is noted that the amplitude peaks occurred before the flare flux peaks. The mechanism of this phenomenon has not been clearly understood. According to the work [29, 30], the time delay is needed for the D-region recombination - ionization processes which recover the balance under the enhancement of X-ray flare. This time delay an important key to solve the continuity equation of electrons, and thereby identify the responses of D-region of the ionosphere to the solar flares. Figure 24 shows that result is in accordance with the result of Kumar who observed the responses of VLF signal to solar flares in six months of 2007 at Suva and found that the variation of amplitude of VLF signal related to the X-ray intensity with the logarithmic function [31]. If we know this relationship, we can predict the strong solar events by detecting the VLF perturbations (Table 3) when the GOES detectors are saturate to lead to uncertainly obtain the correct values of the peak X-ray flux [26, 27, 29].
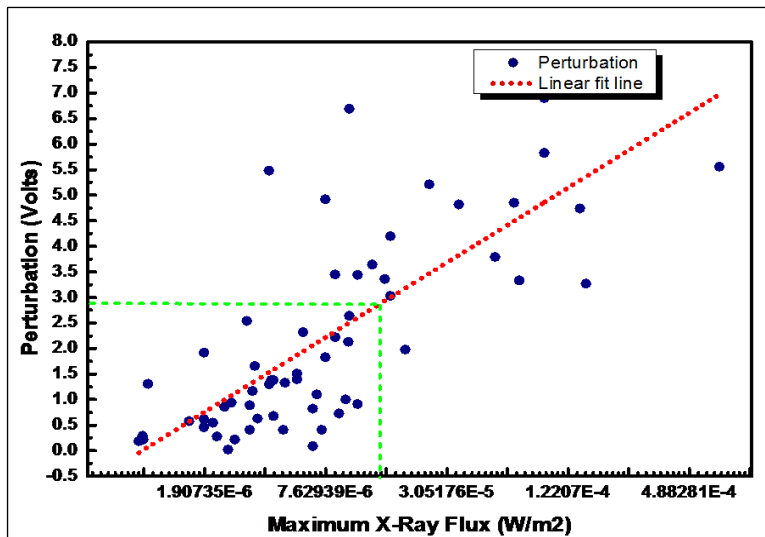
Fig. 24: *Amplitude Perturbations of NWC Signal as a Function of X-Ray Flux Recorded at Khatav for the Year 2011.*

Table 3: *VLF Perturbations Due to Solar Flares During the Period 2009–2012.*

Date	VLF (Min) (Volts)	VLF (Max) (Volts)	ΔV	X-ray Flare Class	X-ray Flare Energy (W/m^2)
22-12-2009	1:23	4:56	3.29	C7.2	7.2 x 10^{-6}
23-12-2009	-2.17	-0.78	1.39	C6.4	6.4 x 10^{-6}
15-01-2010	1:23	4:56	3.29	C7.2	7.2 x 10^{-6}
18-01-2010	-2.17	-0.78	1.39	C6.4	6.4 x 10^{-6}
19-01-2010	0.27	0.37	0.1	C1.3	1.3 x 10^{-6}

Research & Reviews: Journal of Space Science & Technology
Volume 6, Issue 3
ISSN: 2321-2837 (Online), ISSN: 2321-6506 (Print)

STM JOURNALS

19-01-2010	1:49	2:02	0.53	B8.4	8.4×10^{-7}
19-01-2010	1.66	1.76	0.1	B5.8	5.8×10^{-7}
19-01-2010	1.57	1.73	0.16	B8.3	8.3×10^{-7}
20-01-2010	0.94	2.94	2	C5.2	7.2×10^{-6}
20-01-2010	5.03	6.54	1.51	M1.7	1.7×10^{-5}
20-01-2010	-2.44	-1.89	0.55	C4.0	4.0×10^{-6}
20-01-2010	1.13	3.83	2.7	C5.0	5.0×10^{-6}
20-01-2010	1.61	3.67	2.06	C3.9	3.9×10^{-6}
20-01-2010	1.95	2.83	0.88	C3.1	3.1×10^{-6}
20-01-2010	2.42	5.33	2.91	C9.7	9.7×10^{-6}
20-01-2010	3.54	5.96	2.42	M1.6	1.6×10^{-5}
27-03-2010	-0.84	-0.89	0.05	C3.7	3.7×10^{-6}
27-03-2010	-3.55	-0.32	3.23	M1.8	1.8×10^{-6}
27-03-2010	2.77	3.2	0.43	C1.2	1.2×10^{-6}
12-06-2010	2.72	3.22	0.5	C2.0	2×10^{-6}
12-06-2010	0.66	0.76	0.1	C1.5	1.5×10^{-6}
13-06-2010	2.36	3.08	0.72	C1.0	1×10^{-6}
13-06-2010	1.44	3.11	1.67	C6.1	6.1×10^{-6}
13-06-2010	1.42	1.97	0.55	B4.6	4.6×10^{-7}
13-06-2010	3.26	6.08	2.82	M1.0	1×10^{-5}
13-06-2010	2.08	2.97	0.89	C1.2	1.2×10^{-6}
9-07-2010	2.8	3.1	0.3	C1.2	1.2×10^{-6}
27-07-2010	2.28	2.36	0.08	C1.2	1.2×10^{-6}
18-08-2010	0.92	1.12	0.2	C1.8	1.8×10^{-6}
15-12-2010	2.26	3.13	0.87	C2.2	2.2×10^{-6}
4-01-2011	-0.66	0.04	0.62	C1.9	1.9×10^{-6}
4-01-2011	0.86	1.15	0.29	B9.4	9.4×10^{-7}
14-01-2011	-1.51	0.41	1.92	C1.6	1.6×10^{-6}
21-01-2011	0.24	1.41	1.17	C3.3	3.3×10^{-6}
21-01-2011	0.88	1.10	0.22	B9.5	9.5×10^{-7}
22-01-2011	0.37	1.23	0.86	C2.4	2.4×10^{-6}
9-02-2011	-2.46	-0.48	1.98	M1.9	1.9×10^{-5}
10-02-2011	0.97	1.43	0.46	C1.9	1.9×10^{-6}
10-02-2011	1.07	1.62	0.55	C2.1	2.1×10^{-6}
11-02-2011	-0.51	-0.32	0.19	B9.0	9.0×10^{-7}
15-02-2011	-1.76	5.85	7.61	X2.2	2.2×10^{-4}
15-02-2011	0.34	1.67	1.33	C4.8	4.8×10^{-6}
16-02-2011	-2.31	0.33	2.64	M1.0	1×10^{-5}
16-02-2011	1.10	3.42	2.32	C5.9	5.9×10^{-6}
16-02-2011	1.25	1.53	0.28	C2.2	2.2×10^{-6}
16-02-2011	0.86	4.3	3.44	M1.1	1.1×10^{-5}
16-02-2011	-0.35	-2.48	2.13	C9.9	9.9×10^{-6}
16-02-2011	-1.84	-1.43	0.41	C3.2	3.2×10^{-6}
16-02-2011	-4.55	-3.24	1.31	C1.0	1×10^{-6}
16-02-2011	-5.02	-1.99	3.03	M1.6	1.6×10^{-5}

18-02-2011	1.12	6.60	5.48	C4.0	4 x 10⁻⁶
18-02-2011	1.38	4.83	3.45	C8.5	8.5 x 10⁻⁶
18-02-2011	1.37	3.20	1.83	C7.6	7.6 x 10⁻⁶
18-02-2011	0.29	0.97	0.68	C4.2	4.2 x 10⁻⁶
18-02-2011	-0.45	4.40	4.85	M6.6	6.6 x 10⁻⁵
19-02-2011	-0.56	1.10	1.66	C3.4	3.4 x 10⁻⁶
19-02-2011	1.31	2.25	0.94	C2.6	2.6 x 10⁻⁶
19-02-2011	1.27	3.49	2.22	C8.5	8.5 x 10⁻⁶
24-02-2011	1.13	5.95	4.82	M3.5	3.5 x 10⁻⁵
27-02-2011	0.32	1.70	1.38	C4.2	4.2 x 10⁻⁶
8-03-2011	-0.82	2.82	3.64	M1.3	1.3 x 10⁻⁵
8-03-2011	0.66	4.02	3.36	M1.5	1.5x 10⁻⁵
8-03-2011	1.53	2.93	1.4	C5.5	5.5 x 10⁻⁶
8-03-2011	0.25	0.66	0.41	C4.7	4.7 x 10⁻⁶
8-03-2011	-1.29	2.5	3.79	M5.3	5.3 x 10⁻⁵
9-03-2011	1.12	2.42	1.3	C4.0	4 x 10⁻⁶
9-03-2011	-1.68	-1.27	0.41	C7.3	7.3x 10⁻⁶
9-03-2011	-4.45	0.47	4.92	C7.6	7.6x 10⁻⁶
9-03-2011	-2.28	0.99	3.27	X1.5	1.5 x 10⁻⁴
30-07-2011	-1.62	5.28	6.9	M9.3	9.3x 10⁻⁵
3-08-2011	-0.50	6.19	6.69	M1	1 x 10⁻⁵
3-08-2011	0.94	4.27	3.33	M7	7 x 10⁻⁵
3-08-2011	0.26	2.80	2.54	C3.1	3.1 x 10⁻⁶
4-08-2011	-3.41	-2.83	0.58	C1.6	1.6 x 10⁻⁶
4-08-2011	-1.31	-0.42	0.89	C3.2	3.2 x 10⁻⁶
4-08-2011	0.28	6.11	5.83	M9.3	9.3 x 10⁻⁵
4-08-2011	0.21	0.84	0.63	C3.5	3.5x 10⁻⁶
4-08-2011	-1.03	-1.05	0.02	C2.5	2.5 x 10⁻⁶
9-08-2011	0.09	5.30	5.21	M2.5	2.5 x 10⁻⁵
9-08-2011	0.58	6.23	5.56	X6.9	6.9 x 10⁻⁴
22-09-2011	0.37	1.19	0.82	C6.6	6.6 x 10⁻⁶
22-09-2011	1.0	1.09	0.09	C6.6	6.6 x 10⁻⁶
22-09-2011	1.05	1.78	0.73	C8.9	8.9 x 10⁻⁶
22-09-2011	0.46	1.37	0.91	M1.1	1.1 x 10⁻⁵
22-09-2011	0.38	5.12	4.74	X1.4	1.4 x 10⁻⁴
22-9-2011	-2.62	-1.24	1.51	C5.5	5.5 x 10⁻⁶
22-9-2011	-2.75	-1.24	1.38	C4.1	4.1 x 10⁻⁶
23-09-2011	-2.1	-1.10	1	C9.6	9.6 x 10⁻⁶
23-09-2011	-0.97	3.23	4.2	M1.6	1.6 x 10⁻⁵
23-09-2011	0.03	0.25	0.22	C2.7	2.7 x 10⁻⁶
23-09-2011	0.22	1.32	1.1	C6.9	6.9 x 10⁻⁶
11-01-2012	-0.65	0.66	1.31	C3.7	3.7x 10⁻⁶
12-01-2012	-0.63	0.22	0.85	C2.5	2.5 x 10⁻⁶
17-01-2012	-0.73	1.85	2.58	M1.0	1 x 10⁻⁵
23-01-2012	-4.29	-3.00	1.29	C1.9	1.9x 10⁻⁶

| 23-01-2012	-2.94	0.40	3.34	M8.7	8.7 x 10^{-5}
26-01-2012	-4.12	-3.28	0.84	C5.8	5.8 x 10^{-6}
26-01-2012	-3.55	-1.44	2.11	C7.9	7.9 x 10^{-6}
26-01-2012	-1.19	0.97	2.16	C5.2	5.2 x 10^{-6}
27-01-2012	-1.41	-0.86	0.55	C2.1	2.1x 10^{-6}
27-01-2012	-0.58	1.05	1.63	C5.5	5.5x 10^{-6}
27-01-2012	-5.69	2.31	8	X1.7	1.7 x 10^{-4}
7-02-2012	-1.09	0.04	1.13	C1.7	1.7x 10^{-6}
8-03-2012	-2.26	-0.74	1.52	C7.2	7.2x 10^{-6}
9-03-2012	-1.77	2.74	4.51	M6.3	6.3 x 10^{-5}
7-05-2012	-0.78	2.33	3.11	C7.1	7.1 x 10^{-6}
7-05-2012	0.63	1.13	0.5	C2.7	2.7 x 10^{-6}
7-05-2012	0.84	1.8	0.96	C4.0	4 x 10^{-6}
16-05-2012	-0.47	-0.14	0.33	C2.5	2.5 x 10^{-6}
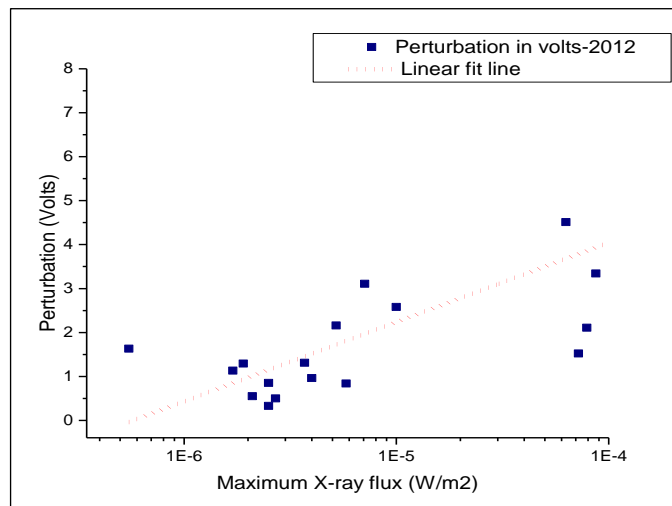
Fig. 25: *Amplitude Perturbations of NWC Signal as a Function of X-ray Flux Recorded at Khatav for the Year 2012.*
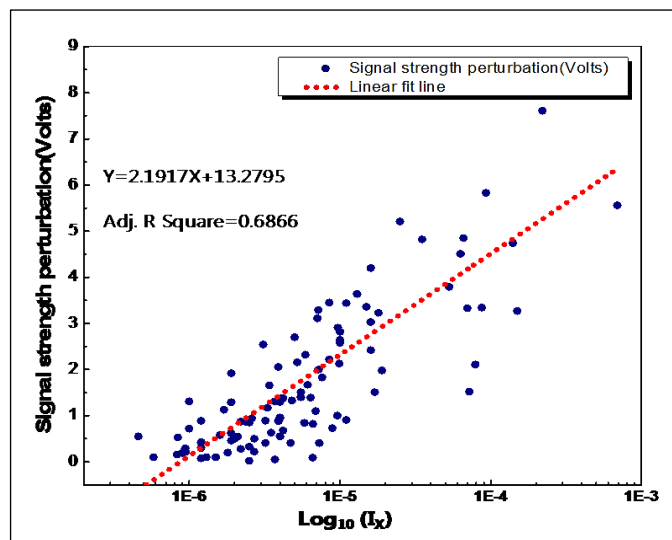

Fig. 26: *Amplitude Perturbations of NWC Signal as a Function of X-ray Flux Recorded at Khatav (2009–2012). The Dotted Line is the Fitted Straight Line for Those Data Points.*

Therefore, it can be concluded that the VLF technique is useful to detect the SID and understand the physics processes and chemical mechanism of ionospheric D- region.

Figure 24 shows amplitude perturbations of NWC signal as a function of X-ray flux recorded at Khatav for the year 2011. The dotted line is the fitted straight line for those data points. From Figure 24, Y = 2.4318 + 14.66 is the fitting line for the year 2011. In this function, Y means the amplitude perturbations $(A-A_0)$. A is the value of the peaks of amplitude perturbations and A_0 is the unperturbed values of amplitude, X presents the logarithm of the peaks of X-ray flux, R_2 is a statistical measure of how well the regression line approximates the real data points. $R_2 = 0.5776$ shows that 57.76 % of the total variation in y could be explained by the linear relationship between X and Y. From Figure 25, $Y=1.8051X+11.2631$ is the fitting line for the year 2012. $R_2 = 0.4479$. Figure 26 shows amplitude perturbations of NWC signal as a function of X-ray flux recorded at Khatav (2009–2012). The dotted line is the fitted straight line for those data points. Y = 2.1917 + 13.2795 is the fitting line. In this function, Y means the amplitude perturbations $(A - A_o)$. A is the value of the peaks of amplitude perturbations and A_o is the unperturbed values of amplitude, X presents the logarithm of the peaks of X-ray flux, R2 is a statistical measure of how well the regression line approximates the real data points. $R2 = 0.6866$ shows that 68.66% of the total variation in y could be explained by the linear relationship between x and y.

CONCLUSIONS

VLF amplitude of the NWC Cape North transmitter operating at 19.8 kHz and NAA Cutler transmitter, USA operating at 24 kHz recorded by the field strength monitoring system at Khatav (India) have been analyzed for about 150 solar X-ray flare events, during the period July 2009 to May 2012. For the case of signal strength of NWC (19.8 kHz) received by the VLF field strength monitoring system transmitted over sea water varies according to the strength of solar flares that are monitored by GOES-12 satellite. The results arrived at allow for the classification of solar X-ray flares by their effect on the lower ionosphere and indicate the possible mechanisms of VLF propagation in perturbed conditions.

The VLF field strength enhancement take place as the signal penetrates the D-layer thatis undergoing ionization redistribution and electron density increases so the upper boundary of the waveguide drifts slightly downwards to lower heights. During the period from July 31, 2009 to May 16, 2012, the average enhancement ofVLF signal strength of NWC signal (19.8 kHz) for observed 8 B-class flares is calculated to be equal to 0.36 Volts. For C, M and X class flares, the corresponding enhancement is signal strength is observed to be equal to 1.258, 3.4 and 5.836 Volts respectively. Recording the perturbations of the great path NWC (19.8 kHz) from Australia to Khatav, India due to the solar flares during August 2009 to May 2012, it is seen that VLF receiver is sensitive to identify the flare classes A8-class to -X6.9 class.

C flare classes often occurred with 65 % of the total of detected solar flare events. The peaks of the amplitude perturbations of VLF signal occurred after the peaks of X-ray flux radiated by solar flares with the time delay of 1–15 minutes. The enhancement of VLF signal strength is directly proportional to the logarithmic function of the maximum value of the X-ray flux. The results investigate that the effects of X-ray flux on the D-region of ionosphere become more significant than that of the cosmic rays and Lyman-α emission during the solar flare events. The enhancement of the electron density, due to sudden bombardment of X-ray radiation which leads to increase the magnitudes of VLF signals strength. It is observed that receiver at Khatav in India and VLF transmitter at NWC Australia remain in daylight for many hours so SID is observed clearly and enhancement in signal strength is high up to 9 Volts as the discontinuity at the day-night terminator disrupts the signal propagation.

It is also observed that, when receiver at Khatav in India is in daylight, then and VLF transmitter at NAA, USA remain in night for many hours so SID is not so nicely observed

as that of NWC case and enhancement in signal strength is up to 2 to 3 Volts. The signal enhancement for NWC (19.8 kHz) is more than that of NAA (24 kHz) as higher frequencies in the VLF range penetrate into the D-region and will experience greater attenuation over the extended path length. SID modified VLF signal strength would directly relate to the increase of X-ray flux. The amount of X-ray radiation received at the earth should directly correlate to the amount of photoionization in the ionosphere creating higher electron densities in the D-region. The enhanced TEC in the D-region increases its conductivity and the reflection of the radio waves occurs at lower altitudes without experiencing as much atmospheric attenuation. This phenomenon was clearly expressed by the data acquired. Observatory showing a linear correlation between received signal strength and flare magnitude.

It is well known that the ionosphere varies with diurnally and seasonally depending on the amount of direct sunlight received at the top of the atmosphere. The height of the ionosphere is lower in summer and during the day and electron densities are higher. With this, it was expected that SID strength might also vary by season. This was clearly seen in the NWC data where the enhancement of VLF signal strength in the summer was more than that seen in the winter months. The signal strength perturbation of NWC signal is a function of X-ray flux and the enhancement of VLF signal strength relates to the logarithmic function of the peaks of X-ray intensity.

AKNOWLEDGEMENTS

REFERENCES

1. Cliver EW, Dietrich WF. The 1859 Space Weather Event Revisited: Limits of Extreme Activity. J. Space Weather Space Clim. 2013; 3: 1–15p.
2. Halder D. International Journal of Electronics Communication and Computer Engineering 5 2249M and X Class Flares During 2011 to 2013 and their Connection to Auroral Electrojet Indices. 2014; 1–5p.
3. Bond P. Exploring the Solar System John Wiley & Sons, New York. 2012; 462p.
4. solar-center.stanford.edu/SID/docs/SID_Manual.pdf
5. Gopalswamy N. Ground level enhancement events of Solar cycle 23. *Indian Journal of Radio & Space Physics*. 2010; 39: 240–248p.
6. Astrophysical Aspects in the Studies of Solar Cosmic rays. *International Journal of Modern Physics*. 2008; 23: 1–141p.
7. Parker E. Solar Magnetism: Discovery and Investigation, Spatium, Association Pro ISSI 2008; 22: 1–16p.
8. Marhavilas PK. Recorder an official publication of the Canadian Society of Exploration. *Geophysicists*. 2004; 29.
9. http://static.egu.eu/static/12056/newsletter/eggs/eggs_19.pdf
10. Grubor DP, Sulic DM, Zigman V. Classification of X-ray solar flares regarding their effects on the lower ionosphere electron density profile. *Annals of Geophysics*. 2008; 26: 1731–1740p.
11. Wait JR, Spies KP. Characteristics of the Earth- Ionosphere waveguide for VLF Radio waves. National Bureau of Standards Library, Boulder, Colorado. 1965; 300.
12. http://solar-center.stanford.edu/SID/StudentWork/SophieMurray.pdf
13. Thomson NR, Rodger CJ, Clilverd MA. Daytime D region parameters from long-path VLF phase and amplitude. 2011L 116: 1–12p.
14. Ferguson JA, Snyder FP. Approximate VLF/LF Waveguide mode conversion model -*Computer Applications*. 1080; 400: 34p.
15. Chubb et al. Lyman Alpha and X-Ray Emissions during a Small Solar Flare.

Journal of Geophysical Research. Sep 1957; 62(3): 389–398p.

16. Gruber et al. Classification of X-ray Solar Flares Regarding their Effects on the Lower Ionosphere Electron Density Profile. Ann. Geophys. 2008; 26: 1731–1740p.

17. Grubor D., Sulic D., & Zigman V, Influence of Solar X-ray Flares on the Earth-Ionosphere Waveguide, Serbian Astronomical Journal, 171[2005]29-35.

18. solar-center.stanford.edu/SID/StudentWork/LeandraMerola.pdf

19. https://stereo.gsfc.nasa.gov/classroom/EUVsun.shtml

20. Zigman V, Grubor D, Sulic D. D-region electron density evaluated from VLF amplitude time delay during X-ray solar flares. *Journal of Atmospheric and Solar-Terrestrial Physics.* 2007; 69: 775–792p.

21. Jones SL. Solar flares: investigations and selected research, Nova Science Publishers, Inc, New York, 2016.

22. Libo et al. Some Investigations on the Ionosphere during 2012–2014 in China. Space Science Activities in China. 138–155p.

23. Rice DD, Hunsucker RD, Eccles JV, Sojka JJ, Raitt JW, Brady JJ. Characterizing the lower ionosphere with a space - weather - aware receiver matrix. Radio Science Bulletin. 2009; 328: 20– 32p.

24. Zlotnicki J. Li F, Parrot M. Ionospheric Disturbances Recorded by DEMETER Satellite over Active Volcanoes: From August 2004 to December 2010. International Journal of Geophysics. 2013; 17p.

25. Effects of solar X-ray flares in the E region ionosphere of Mars: First model results. Journal of Geophysical Research Space Physics. AGU Publications. 2012; 5: 117p.

26. Tan ML, Tuyen KT. Observation of the effects of solar flares on the NWC signal using the new VLF receiver at Tay Nguyen University. *Sun and Geosphere.* 2014; 8: 27p.

27. Tan ML, Ha TQ, Marbouti M. Study of solar flare induced D-region ionosphere changes using VLF amplitude observations at a low latitude site. *Indian Journal of Radio and Space Physics.* 2014; 43: 197–204p.

28. Maurya AK. ELF/VLF Wave studies of Ionosphere and Magnetosphere Electromagnetic phenomenon in Low latitude region, Ph. D Thesis, IIG, Mumbai, 2013.

29. Kumar A, Kumar S. Space weather effects on the low latitude D-region ionosphere during solar minimum. *Earth, Planets and Space.* 2014; 66: 1–10p.

30. Matthieu Kretzschmar, Thierry Dudok de Wit, Werner Schmutz, Sabri Mekaoui, Jean-François Hochedez, Steven Dewitte. The effect of flares on total solar irradiance. *Nature Physics.* 2010; 6: 690–692p.

31. Mohd Masri Abd Rashid, Mahamod Ismail, Zamri Zainal Abidin. Preliminary Results of Solar Flare Induced D-Region Perturbations over UKM Using Stanford AWESOME Receiver. *Journal of Applied Mathematics and Physics.* 2015; 3: 455–464p.

Cite this Article
A.K. Sharma, C. T. More. Effect of Solar X-ray Flares on VLF Radio Wave Signal Strength at 19.8 and 24 kHz Received at Khatav (India) (16°46'N, 75°53'E). *Research & Reviews: Journal of Space Science & Technology.* 2017; 6(3): 15–34p.